Methods xxx (2017) xxx–xxx

Contents lists available at ScienceDirect

Methods

journal homepage: www.elsevier.com/locate/ymeth

A novel method for quantitative measurements of gene expression in single living cells

A. Mandic, D. Strebinger, C. Regali, N.E. Phillips, D.M. Suter *

The Institute of Bioengineering (IBI), School of Life Sciences, Swiss Federal Institute of Technology Lausanne (EPFL), 1015 Lausanne, Switzerland

ARTICLE INFO

Article history:
Received 13 December 2016
Received in revised form 12 March 2017
Accepted 14 April 2017
Available online xxxx

Keywords:
mRNA half-life
Protein synthesis rate
Absolute protein number quantification
Single cell analysis
Luminescence microscopy

ABSTRACT

Gene expression is at the heart of virtually any biological process, and its deregulation is at the source of numerous pathological conditions. While impressive progress has been made in genome-wide measurements of mRNA and protein expression levels, it is still challenging to obtain highly quantitative measurements in single living cells. Here we describe a novel approach based on internal tagging of endogenous proteins with a reporter allowing luminescence and fluorescence time-lapse microscopy. Using luminescence microscopy, fluctuations of protein expression levels can be monitored in single living cells with high sensitivity and temporal resolution over extended time periods. The integrated protein decay reporter allows measuring protein degradation rates in the absence of protein synthesis inhibitors, and in combination with absolute protein levels allows determining absolute amounts of proteins synthesized over the cell cycle. Finally, the internal tag can be excised by inducible expression of Cre recombinase, which enables to estimate endogenous mRNA half-lives. Our method thus opens new avenues in quantitative analysis of gene expression in single living cells.

1. Introduction

The past decades have witnessed impressive developments in methods allowing quantitative analysis of gene expression at the mRNA and protein levels, such as RNA-seq and mass spectrometry. However, these methods often require large number of cells and results are often difficult to extrapolate to individual cells because of population heterogeneity. Even in phenotypically homogeneous cell populations, the copy numbers of mRNAs and proteins change over time and vary from cell to cell. This variability has been shown to be caused by various parameters such as differences in cell cycle phase [1,2], position of a cell within a colony [3], and intrinsic noise of biochemical reactions that lead to gene expression stochasticity [4]. Recently, methods allowing transcriptome-wide measurements of gene expression in single cells have been developed [5,6]. Nevertheless, most of them only permit qualitative assessment of gene expression since they typically suffer from low recovery and biases due to exponential amplification of a few mRNA molecules, or are hampered by the requirement of expensive equipment and technical challenges [6]. On the protein level, recent single-cell mass spectrometry experiments allowed quantification of translational heterogeneity during development [7,8]. However, these methods provide only a snapshot of gene and protein expression at a given time point since they require cell fixation or lysis. To directly measure dynamical changes of transcriptional activity in single living cells, different approaches have been developed. Using the MS2 or PP7 system, transcriptional fluctuations and dynamics of transcriptional activation have been studied over time [9–12]. In addition, short-lived luciferase reporters have also been used in order to describe transcriptional kinetics in single living mammalian cells [13]. While these methods are limited to the investigation of one gene at a time, their sensitivity and the possibility to calibrate them allows calculating absolute transcript numbers in single living cells over time. To quantify absolute levels and temporal fluctuations of endogenous proteins, fluorescent proteins can be used as a tag [14–18]. Moreover, other single-molecule techniques have been used in *E. coli* and *S. cerevisiae* to robustly determine protein copy numbers in different compartments of single living cells [19]. Still, in mammalian cells the sensitivity of fluorescent reporters is limited to the detection of several thousands of molecules per cell because of their strong autofluorescence, while imaging over extended periods of time with high temporal resolution are restricted due to fluorescence phototoxicity [18,20].

Absolute expression levels of protein and mRNA are determined both by their respective synthesis and degradation rates. These parameters are generally not directly measurable, and studies assessing them have been mainly using drugs blocking transcription or translation [21–23]. Since these drugs globally interfere

* Corresponding author at: Ecole Polytechnique Fédérale de Lausanne, FSV-IBI-UPSUTER, Station 19, 1015 Lausanne, Switzerland.
E-mail address: david.suter@epfl.ch (D.M. Suter).

http://dx.doi.org/10.1016/j.ymeth.2017.04.008
1046-2023/

with gene expression, cell physiology suffers major perturbations and thus protein and mRNA degradation pathways can be severely perturbed [23–25].

Here we describe a method based on excisable, internal central dogma (CD) tagging of random endogenous proteins with a highly sensitive luminescence reporter and a protein decay reporter. This approach enables measuring absolute protein levels at high temporal resolution, mRNA and protein half-lives without the use of drugs inhibiting transcription or translation, as well as inferring absolute protein synthesis rates in single living cells (Fig. 1).

2. Material and methods

2.1. DNA constructs

2.1.1. Construction of the SA-Nluc-Bsd-SNAP-SD (NBS) lentivector

To assemble the SA-Nluc-Bsd-SNAP-SD fragment, the coding sequence for Nanoluc (Nluc) was amplified by PCR with a forward primer flanked by an NheI restriction site, and a reverse primer flanked by an EcoRI restriction site. The coding sequence encoding Blasticidin resistance (Bsd) was amplified with a forward primer flanked by an EcoRI restriction site, and a reverse primer flanked by a ClaI restriction site. Both fragments were digested with the corresponding restriction enzymes and ligated together and into the NheI-ClaI cut pSTAR lentiviral vector [26]. The Nluc-Bsd sequence was then PCR-amplified with a forward primer flanked by an XbaI restriction site and a splice acceptor (SA) and a reverse primer flanked by an XhoI restriction site. The SNAP coding sequence was PCR-amplified with a forward primer flanked by an XhoI restriction site and a reverse primer flanked by a splice donor (SD) and a ClaI restriction site. The SA-Nluc-Bsd and the SNAP-SD fragments were digested with the corresponding restriction enzymes and ligated into an NheI-ClaI cut plasmid. Finally, the SA-Nluc-Bsd-SNAP-SD was PCR-amplified with a forward primer flanked by a LoxP site and an NheI restriction site, and a reverse primer flanked by a LoxP site and a ClaI restriction site. This fragment was then ligated into the NheI-ClaI cut pSTAR lentiviral vector.

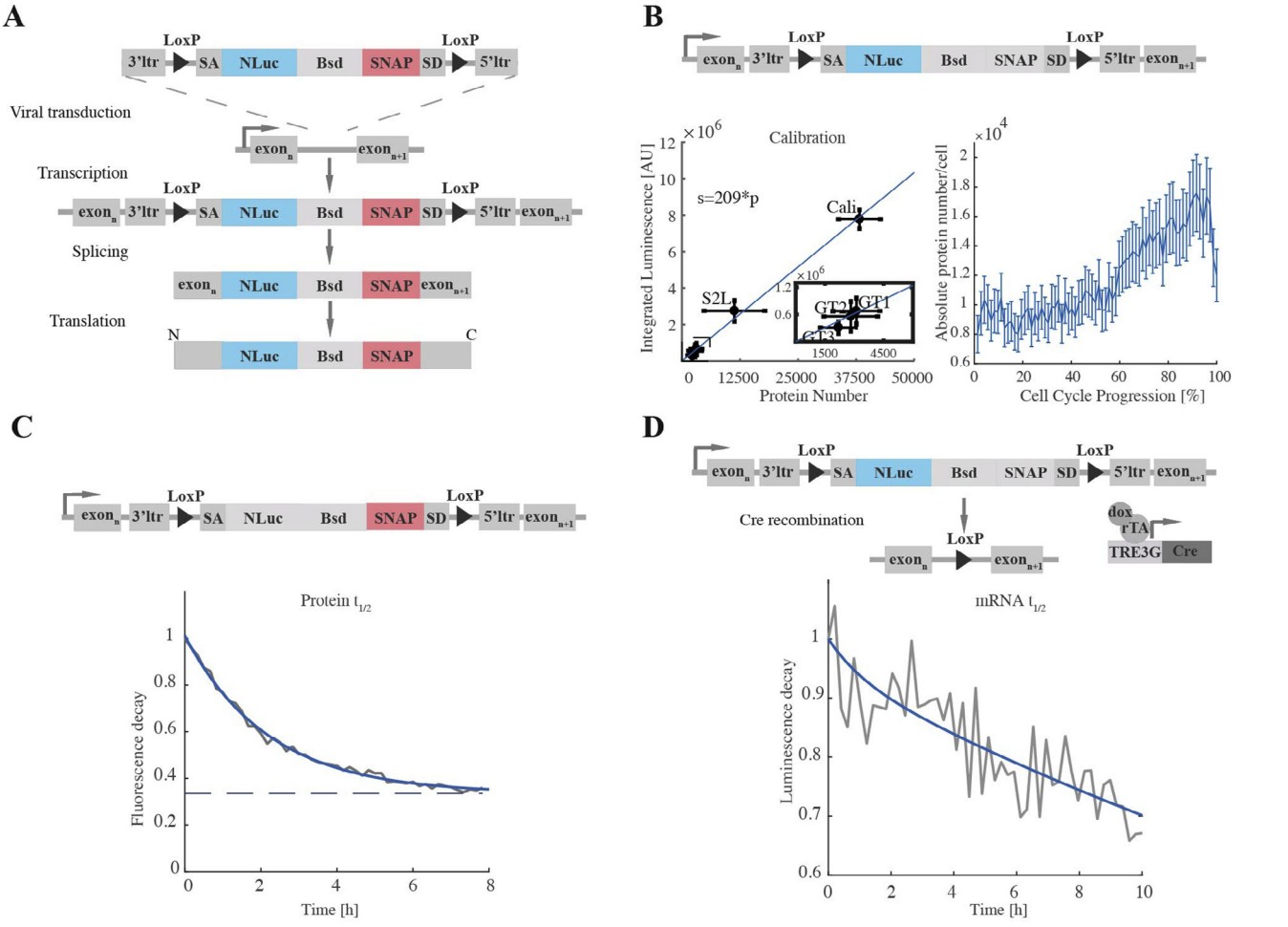

Fig. 1. (A) Generation of CD-tagged cell lines. The fusion construct encoding NanoLuc luciferase (Nluc), blasticidin deaminase (Bsd) and SNAP-tag was randomly inserted into the genome of ES cells by lentiviral transduction. The construct is flanked by splice donor (SD) and splice acceptor (SA) sites, allowing its retention as a new exon after splicing of the mRNA, leading to an internally labeled protein with Nluc and SNAP-tag. (B) Monitoring of protein fluctuations during the cell cycle. Imaging of the Nluc signal allows observation of protein level fluctuations in single cells at high time resolution (right panel). The calibration inset illustrates the linear correlation between protein copy numbers per cell (x-axis) with the integrated Luminescence intensity recorded in the microscope (y-axis). Each point represents the mean protein number (x-axis) and the corresponding mean integrated luminescence intensity (y-axis) of each cell line (at least two replicates per cell line). The inset shows a magnification in the lower range of the diagram. Error bars: SD. (C) Determination of protein half-lives. To observe degradation of the CD-tagged proteins, SiR-SNAP pulse-labeled cells are monitored by fluorescence time-lapse imaging. (D) Determination of mRNA half-life. The two loxP sites flanking the lentiviral construct allow its excision upon dox-induced expression of Cre recombinase, leading to the decay of the luminescent signal that depends on both protein and mRNA half-lives. Knowing the protein half-life, mRNA half-life can be directly calculated from these traces. All plots in the scheme are taken from data generated with the U2SURP cell line.

Please cite this article in press as: A. Mandic et al., Methods (2017), http://dx.doi.org/10.1016/j.ymeth.2017.04.008

2.1.2. Construction of the pLV-PGK-rtTA3G-IREShygro lentivector

The rtTA3G (reverse Tetracycline Transactivator third generation) expression construct was generated by excising the rtTA3G coding sequence from pLV-pGK-rtTA3G-IRES-Bsd [26] using AgeI and EcoRI. Next, the IREShygro cassette was amplified with a forward primer flanked by an MfeI site and a reverse primer flanked by a SalI site. Subsequently, the PCR product was digested and the two resulting fragments were ligated. The ligated product was used for a subsequent round of PCR amplification using a forward primer flanked by an AgeI site and a reverse primer flanked by a SalI site, and the resulting PCR product was digested with the aforementioned enzymes. The rtTA3G-IREShygro cassette was then ligated into the AgeI/SalI-digested pLV-pGK-rtTA3G-IRES-Bsd.

2.1.3. Construction of pLV-pGK-NLuc-Fluc-NLS-P2A-H2B-mCherry-IRES-Hygro

To generate the lentiviral construct for the stable expression of an NLuc-Fluc-NLS fusion protein and H2B-mCherry for identification of the positive cells, pLV-PGK-rtTA3G-IREShygro was digested with BamHI and SalI and an annealed oligo pair encoding the co-translationally cleaved P2A peptide [27] was inserted. The coding sequences for Nluc and Fluc-NLS were fused in frame and inserted into the pLVTRE3GMCS lentiviral vector [26]. Next, NLuc-Fluc-NLS was amplified from pLV-TRE3G-NLuc-Fluc-NLS by PCR with a forward primer flanked with a BamHI site and a reverse primer flanked by a ClaI site, and the resulting fragment was ligated into the digested pLV-P2A-IRES-Hygro. Finally, an H2B-mCherry cassette was amplified with a forward primer flanked by an XbaI site and a reverse primer flanked by an XmaI site. The PCR product was digested and ligated into the pLV-GK-NLuc-Fluc-NLS-P2A-IRES-Hygro using XbaI and XmaI.

All constructs were verified by Sanger sequencing

2.2. Cell culture

The E14 embryonic stem cell line (kindly provided by Didier Trono, EPFL) was used for all experiments. Cells were cultured on dishes coated with 0.1% gelatin type B (Sigma), in GMEM (Sigma) supplemented with 10% ES-cell qualified FBS, 1× nonessential amino acids (NEAA), 2 mM L-glutamine, sodium pyruvate, 100 mM 2-mercaptoethanol, penicillin and streptomycin, leukemia inhibitory factor (LIF), CHIR99021 at 3 μM and PD184352 at 0.8 μM and passaged every 2–3 days. CD-tagged cell lines were maintained in selection while culturing with 8 μg/ml of blasticidin and 2 μg/ml of puromycin, and the calibration cell line was maintained in selection with 40 μg/ml of hygromycin.

2.3. Lentiviral vector production and generation of stable cell lines using central dogma (CD) tagging

To measure protein level dynamics and expression parameters such as protein half-life, mRNA half-life and protein synthesis rate, we have developed a method based on CD-tagging [15,28,29]. Briefly, we used lentiviral transduction to randomly integrate our reporter into the genome, followed by antibiotic treatment to select for clones having successfully fused the reporter to an endogenously expressed protein (Fig. 1A). Lentiviral vector production was performed by co-transfection of HEK 293T cells with the lentiviral construct, the envelope (PAX2) and packaging (MD2G) constructs using calcium phosphate, and concentrated 120-fold by ultracentrifugation as described previously [13]. CD-tagged cell lines were generated by infecting E14 cells with the concentrated virus carrying the NBS construct. The cells were seeded at a density of 40,000 cells per 10 cm dish and transduced at low multiplicity of infection (MOI), in order to generate cell lines with only one construct insertion. Antibiotic selection was carried out by addition of 8 μg/ml of blasticidin 48 h after transduction. The outgrown colonies were picked 10 days after transduction. In order to introduce the construct carrying the Cre-recombinase gene, CD-tagged cell lines were seeded at density of 50,000 cells per well of a 6-well plate and transduced with 25 μl of pLVTRE3G-Cre and 25 μl of pLV-PGK-rtTA3G-IREShygro concentrated lentiviral vector. Selection was performed by addition of puromycin at 2 μg/ml, 48 h after transduction.

Table 1
List of primers used for 3′RACE insertion site mapping.

List of primers used for 3′ RACE	
OligodT+A	5′ GCTCGCGAGCGCGTTTAAACGCGCACGCGTTTTTTTTTTT TTTTTTTVN 3′
R1	5′ GCTCGCGAGCGCGTTTAAAC 3′
R2	5′ GCGTTTAAACGCGCACGCGT 3′
F1	5′ TCATCAGCTACAGCCACCTG 3′
F2	5′ GAAATCCCGTGCCCATTCT 3′

2.4. Mapping of insertion sites

To identify the mRNA to which the NBS sequence was fused in each CD-tagged cell line, we used 3′ rapid amplification of cDNA ends (3′RACE) to amplify the portion of cDNA between the CD-cassette and the poly(A) tail of the mRNA, as described before [30]. RNA was extracted from cells of each clone using the GenElute Mammalian Total RNA MiniPrep Kit (Sigma). First-strand cDNA was synthetized by SuperScript II reverse transcriptase (Invitrogen) and an oligodT primer with an adaptor sequence (Table 1). The complementary RNA was digested using RNAse H. The cDNAs were then subjected to one round of PCR with a primer specific to the SNAP coding sequence (Table 1, F1) and an anchor primer complementary to the polyA region (Table 1, R1). A second round of PCR was performed using a nested primer on the SNAP coding sequence and an abridged anchor primer (Table 1, F2, R2). The bands from the nested PCR reaction were purified using the QIAquick gel extraction kit (QIAGEN) and directly sequenced using the nested primer (Table 1, F2). Sequences derived from 3′ RACE were used to identify the insertion site using the BLAT genomic alignment tool.

2.5. Live luminescence microscopy and absolute protein quantification

2.5.1. Luminescence microscopy

Luminescence imaging of all cell lines was performed on an Olympus LuminoView LV200 microscope equipped with an EM-CCD camera (Hamamatsu photonics, EM-CCD C9100-13), a 60-fold oil-immersion magnification objective (Olympus UPlanSApo 60x, NA 1.35, oil immersion) in controlled environment conditions (37 °C, 5% CO_2). Cells were seeded on FluoroDishes (WPI, FD35-100) coated with E-Cadherin as previously described for all imaged cell lines [31]. For calibration experiments, the exposure time was adjusted to the brightness of each cell line to avoid signal saturation (between one and five minutes), and three consecutive frames were taken.

For the time-lapse imaging of the CD-tagged clones, images were acquired for 24–48 h. Two days before the experiment, 30,000 cells of the CD-tagged cell line of interest and 3000 calibration cells were mixed and seeded per dish. Luminescent images were then acquired using a 600 nm LP filter (Chroma) for Fluc and 460/36 nm filter (Chroma) for Nluc. To ensure an optimal signal-to-noise ratio and to avoid saturation of the calibration cells in any frame, we used several exposure times for both Fluc and Nluc. Images during time-lapse experiments were acquired as following: a frame in the Fluc channel (exposure time:

45 s–2 min), followed by a frame in the Nluc channel with a short exposure time (1–3 min) followed by another frame in Nluc channel with a longer exposure time (10 min). The first two frames were used for signal normalization and protein number quantification as described later. The 10 min exposure time in the Nluc channel was used for observation of the CD-tagged endogenous protein level fluctuations (Supplementary Mov. 1). Before each movie, these parameters had to be optimized since they depended on Nluc substrate activity and endogenous protein expression levels. For Nluc imaging we used the NanoLuc MT Cell Viability Assay Substrate (Promega) that was diluted 1:1 in DMSO and this mix was diluted 1:2000 in cell culture medium directly after plating to allow equilibration of the substrate until imaging. On the day of recording, the medium was supplemented with 0.5 mM luciferin (NanoLight Technology, Cat#306A) for Fluc imaging.

2.5.2. Calibration of the luminescence microscope for absolute quantification

Another advantage of our highly sensitive luminescence microscopy setup is the linear correlation between light emission and Fluc molecule number [13]. To cover a broad range of Fluc expression levels, we used ES cell lines expressing various levels of Fluc-NLS in the nucleus, generated by i) gene trapping, as described in [13], ii) expression of an Nluc-Fluc fusion protein driven by a PGK promoter using a PGK-Nluc-Fluc lentiviral vector (Cali, this study), and iii) Knock-in of Fluc in fusion to Sox2 [26]. 200,000 cells of each cell line were seeded in duplicates on E-Cadherin coated dishes and imaged the next day on an Olympus LV200 by acquiring three frames at multiple positions in the dish. After image acquisition one dish was used to determine the total number of cells using a cell counting chamber, whereas the other dish was used to perform a Luciferase assay (BrightGlo, Promega, Madison, WI, USA). Known amounts of recombinant Luciferase (QuantiLum recombinant Luciferase, Promega, Madison, WI, USA) were used as standards for the assay (0 pg, 0.524 pg, 3.275 pg, 6.55 pg, 65.5 pg, 196.5 pg and 262 pg) and were diluted into a lysate of 200,000 wild type E14 cells. This allowed us to calculate the total number of Fluc molecules per cell lysate, and we used the number of cells we counted to determine the average protein copy number per cell [13]. A custom CellProfiler pipeline (www.cellprofiler.org) was then used to identify individual cells and to measure their integrated luminescence intensity. The background for the same area was subtracted from the integrated intensity measurements. For each cell line we measured at least 900 individual cells in at least two independent experiments (GT3: 1459 cells, 3 experiments; GT2: 987 cells, 2 experiments; GT1: 1544 cells, 4 experiments; S2L: 947 cells, 2 experiments; Cali: 956 cells, 4 experiments). Finally the mean and the standard deviation of the integrated intensities and the protein numbers per cell were computed and plotted against each other for each cell line. The slope of the resulting calibration curve provides a proportionality constant $\alpha = 1/\text{slope}$, allowing calculation of the number of protein copies from the observed integrated light intensity in the microscope.

2.5.3. Assessment of the cross-talk between Fluc and Nluc channels

The filters described above allow the separation of the emission spectra of Nluc (460/36) and Fluc (700LP). To determine the extent of cross-talk from the Fluc to the Nluc channel and vice versa, we imaged calibration cells with either 0.5 mM Luciferin or 1 µl of 1:1 diluted MT Cell Viability Assay Substrate alone in both channels. While the cross-talk of Fluc to the 460/36 channel was undetectable, 3% of the Nluc signal measured in the 460/36 channel was detected in the 700LP channel. To correct for this, we subtracted 3% of the Nluc signal from the Fluc signal in all subsequent analyses where both protein species are measured in the same cells.

2.5.4. Image processing and calculation of absolute protein numbers

To identify the calibration cells in each frame we used a custom CellProfiler pipeline to segment the Fluc movie, and we measured the luminescence intensity of the identified cells in the Fluc and the Nluc channels. These measurements were subsequently used to calculate the protein copy numbers in each single cell in each frame, using Eq. (1):

$$p_i = \frac{Nluc_i}{tNluc_i} * \alpha * \frac{5 * \left(\overline{Fluc_c} - 0.03 * \frac{tFluc_c}{tNluc_c} * \overline{Nluc_c}\right) * tNluc_c}{tFluc_c * \overline{Nluc_c} * \beta} \quad (1)$$

where p_i is the amount of proteins in the measured cell, α is the proportionality constant of the microscope (defined as 1/slope of the calibration curve), β is the fraction of collected Fluc signal in presence of the 700LP filter, $Nluc_i$ represents the integrated Nluc intensity of the measured cell, $tNluc_i$ is the exposure time in the Nluc channel which was used to measure $Nluc_i$, $\overline{Fluc_c}$ and $\overline{Nluc_c}$ are the mean integrated Fluc and Nluc intensities of the calibration cells in the analyzed frame and $tNluc_c$ and $tFluc_c$ are the exposure times for the Nluc and Fluc channel used to measure the calibration cells, respectively. The factor 5 originates from the 5 min exposure time used for Fluc calibration to absolute protein copy numbers. The assignment of the error to protein copy numbers for each clone is described in Supplementary Information, Section 1.

2.6. Live fluorescence microscopy

Time-lapse fluorescence imaging was performed using an inverted Olympus Cell xCellence microscope equipped with a 20-fold objective (Olympus UPlanSApo 20x, NA 0.75) in controlled environment conditions (37 °C, 5% CO_2) for 24 h. The cells were seeded on E- cadherin as described previously [31] at a density of 20,000 cells per well of a high content imaging 96- well plate (Sigma). Time-lapse imaging was performed in fluorobrite DMEM medium, supplemented with 10% ES-cell qualified fetal bovine serum, 1x nonessential amino acids (NEAA), 2 mM L-glutamine, sodium pyruvate, 100 µM 2-mercaptoethanol, penicillin and streptomycin, leukemia inhibitory factor (LIF), CHIR99021 at 3 µM, PD184352 at 0.8 µM, blasticidin at 8 µg/ml and puromycin at 2 µg/ml. The SiR-SNAP dye was added at a final concentration of 30nM for 30 min and then carefully washed away. Imaging was performed immediately thereafter, in the Cy5 channel (650/13) using a laser power of 80%, every 10 min with an exposure time of 300 ms. The cells were imaged for 24 h and maintained their viability as assessed by their healthy appearance and proliferation throughout imaging (Supplementary Mov. 2).

2.7. Cell tracking

Time-lapse acquisitions of the cell lines of interest were analyzed using the Fiji software. Only the cells that could be easily distinguished from each other were tracked. The outlines were manually drawn around cells, and the shape of the measured area was adjusted if necessary. Background measurements were performed close to every tracked cell in regions devoid of luminescent signal for each frame of the movie. After background subtraction, the integrated intensity was calculated for each measurement and used for further analysis. To monitor protein fluctuations over the cell cycle, cells were tracked from the time they were born (just after division of their mother cell) to the last frame before their division. For easier comparison, all traces were *in silico* synchronized by aligning luminescent traces of each cell between two divisions. In case of SNAP fluorescence and Nluc decay experiments, cells were tracked for 3–10 h, the length of time traces depending on the duration for which a signal was detectable.

2.8. Protein half-life and protein synthesis rate calculation

The protein half-lives were calculated using data from SNAP live fluorescence imaging experiments. For each cell line, 20 cells were tracked for approximately 3–8.5 h, and integrated intensities were calculated after background subtraction. Subsequently, every trace was normalized to the integrated intensity of the first time point so that all decay curves would start with a value of 1. We assumed that protein degradation follows first-order decay kinetics (Eq. (2)), and thus fitted the measured fluorescence intensity data (indicated by N in the equations) using a single exponential fit function to determine the decay rate constant (γ_p) and thus protein half-life ($t_{1/2}$) (Eq. (3)). The constant c in the equation accounts for residual dye fluorescence and cellular autofluorescence.

$$N = N_0 e^{-\gamma_p t} + c \tag{2}$$

$$t_{1/2} = \frac{\ln(2)}{\gamma_p} \tag{3}$$

Since our method allows measuring absolute protein numbers and half-lives of the tagged proteins, we can directly infer the total number of proteins that are degraded per cell cycle (D_T) using Eq. (4):

$$D_T = Ccd * \gamma_p * p_{av} \tag{4}$$

Ccd refers to the cell cycle duration in hours, and p_{av} to the average number of protein copies throughout the cell cycle. Since the net difference between the number of proteins synthesized and the number of proteins degraded over a full cell cycle will be equal to the average number of proteins in early G1 (p_{G1}), we can thus calculate the absolute copy number of proteins synthesized over the cell cycle (S_T):

$$S_T = Ccd * \gamma_p * p_{av} + p_{G1} \tag{5}$$

The error assignment to protein half-lives and synthesis rates is described in Supplementary Information, Sections 2 and 4.

2.9. mRNA half-life calculation

To calculate mRNA half-lives, we took advantage of the possibility to excise the NBS cassette by Cre-mediated recombination. To do so, we first transduced the CD-tagged cell lines with two lentiviral vectors, allowing respectively i) to express the reverse tetracycline transactivator rtTA3G and ii) to express Cre recombinase under the control of an inducible promoter. We then performed time-lapse imaging after dox addition and monitored cells losing their luminescence signal over time (Supplementary Mov. 3). We tracked 20 cells per cell line for 8–10 h, from which we obtained traces whose kinetics are governed by the translation rate of remaining mRNAs, as well as mRNA and protein degradation rates. Each trace was normalized to the absolute protein copy number of the first time point. The measured protein levels (indicated with p in the Eq. (6)) were averaged across all cells and then fitted to the function $p(t)$ given in Eq. (6) [13] to determine the mRNA decay rate constant (γ_m) and thus mRNA half-life ($t_{1/2}$) (Eq. (7)).

$$p(t) = \left(p_0 - \frac{k}{\gamma_p - \gamma_m}\right) e^{-\gamma_p t} + \left(\frac{k}{\gamma_p - \gamma_m}\right) e^{-\gamma_m t} \tag{6}$$

$$t_{1/2} = \frac{\ln(2)}{\gamma_{pm}} \tag{7}$$

We did not use S_T (see Section 2.8) to calculate k (protein synthesis rate multiplied by the initial concentration of mRNA) since protein levels had already started to decrease when we started tracking cells. Thus, we fitted this function to the experimental data of each clone, which allows estimation of k. γ_p was fixed using the value calculated in Section 2.8. p_0 represents the average number of proteins at the beginning of decay curves and was fixed using the initial time point of the averaged data. The assignment of error to mRNA half-lives is described in Supplementary Information, Section 3.

3. Theory

To monitor absolute protein copy number in living cells, we took advantage of the bioluminescent signal emitted by NanoLuc (Nluc), which allows monitoring protein levels and their fluctuations over extended periods of time. Compared to fluorescent reporters, luminescent reporters do not suffer from limitations such as autofluorescence, photobleaching and phototoxicity [18,20]. Therefore, in addition to allowing highly sensitive measurements, the total duration of imaging is only limited by cell survival in a normal culture environment, and the time resolution is only dependent on the signal intensity that sets the lower bound for exposure time. In addition, Nluc is smaller than Firefly Luciferase (Fluc) and fluorescent proteins, and thus it is expected to minimally disturb the structure of the tagged protein. Altogether, this makes Nluc an excellent choice for quantitative protein monitoring in living cells. However, luminescence imaging also has disadvantages such as the need for substrate addition and the still uncommon luminescence microscope systems. Furthermore, the long exposure times required makes it difficult to image multiple positions without sacrificing temporal resolution and results in poor spatial resolution because of cellular/subcellular motions in the second/minute range.

While the substrate of Fluc (luciferin) is stable at 37 °C for several days [32,33], the most widely used substrate of Nluc (furimazine) suffers from instability in cell culture medium at 37° (half-life of ~70 min, data not shown) and shows signs of toxicity at high concentrations (data not shown). Commercially available alternatives are chemically modified versions of Furimazine, which display low to no cell toxicity and rely on cellular processes to become activated. These pro-substrates display a higher stability in culture medium as they become converted to the active form only in the presence of cells. The substrate used in this study (MT Cell Viability Assay Substrate, Promega) relies on the reduction potential of cells to be activated [34]. Consequently, upon addition of the pro-substrate, the concentration of the active form slowly increases over time, followed by plateau phase, and a phase of slow decay. Thus, to account for changes in active substrate concentrations over time, we used a cell line (dubbed Cali) engineered to express an Nluc-Fluc fusion protein allowing us to cross-correlate the current Nluc signal, which suffers from the aforementioned kinetics, to the stable Fluc signal [13]. Additionally, Cali cells express an H2B-mCherry fusion protein, allowing easy identification of these cells by fluorescence imaging. In order to quantify absolute protein numbers, we took advantage of the linear correlation between light emission and Fluc molecule number [13] (Fig. 1B). The obtained calibration curve provides a proportionality constant $\alpha = 1/\text{slope}$, allowing to calculate the number of protein copies from the observed integrated light intensity in the microscope.

Different methods allow measuring protein degradation rates. The most widely used approach is to inhibit translation with drugs such as cycloheximide [22,35]. In this context, protein half-lives can be directly obtained since protein level kinetics are exclusively governed by their degradation rate. However, this approach strongly interferes with normal cellular physiology and thus is only suited to measure relatively short protein half-lives. In contrast, metabolic pulse-chase labeling does not require translational arrest, leading to minimal alteration of normal cell physiology [36–38]. While

these are considered as the gold standard of protein degradation rate measurements, pulse-chase methods are technically challenging and they do not enable real-time measurements at the single cell level. In addition, they are difficult to perform at high time resolution, restricting this approach to the study of long-lived proteins. The recently developed bleach-chase approach allows accurate quantification of protein degradation rates in living cells [39]. This method is based on partial bleaching of endogenous proteins fused to a fluorescent protein, followed by monitoring of fluorescence recovery. While it was shown that partial bleaching causes negligible toxicity, it remains unclear whether this applies to a broad range of cell lines, and the temporal resolution is also limited by the fluorescent tag folding and maturation time [20,39]. In order to overcome these limitations, we decided to exploit the SNAP tag technology to measure protein degradation rates. The SNAP tag has been shown to be a reliable fusion partner that in general does not alter cellular localization, protein function or stability in a large number of fusion proteins [40–45]. To directly observe protein degradation in living cells, cells can be pulse-labeled with the SiR-SNAP dye [40,41], which is not fluorescent unless bound to the SNAP tag (Figs. 1C and 3B). This allows to label only the proteins that were already made at the time of dye addition, and thereby to monitor their degradation over time. Assuming that degradation follows a first order exponential decay, we can calculate protein half-lives as previously described [46]. Therefore, we used a SNAP tag fused to Nluc and to each respective endogenous protein of interest to determine protein degradation rates.

Measuring absolute protein amounts and protein degradation rates directly allows calculating the absolute number of proteins synthesized and degraded during a cell cycle. To infer the absolute number of proteins produced over one cell cycle, one must consider the fact that cells constantly divide. As a consequence, protein levels are not at steady state and synthesis rates must exceed degradation rates on average. Since an early G1 cell gives rise to two early G1 cells after one cell cycle, the absolute excess of proteins made during that time is equivalent to the absolute protein amount of a cell in early G1. Therefore, the absolute copy number of a given protein that a cell has produced per cell cycle can be estimated by calculating the total amount of proteins degraded during one cell cycle, plus the absolute amounts of protein per cell in G1 (see Eqs. (3) and (4), Section 2.8).

The most widely used methods for mRNA degradation rate calculation are based on global transcriptional inhibitors [23], followed by subsequent monitoring of mRNA degradation. These can, however, introduce major perturbations of cell physiology, thereby perturbing mRNA stability [24]. Other approaches such as pulse-labeling by uridine analogs are non-toxic and non-disruptive [24,47,48], but these can suffer from slow incorporation in mRNA and affect cell growth during long-term experiments [24]. Here we took advantage of the possibility to excise the NBS tag from the genomic insertion site through dox-inducible Cre-mediated recombination to quantify mRNA degradation rates (Fig. 1D). Since the kinetics of luminescence decay after NBS excision is governed by already existing mRNAs and proteins in the cells and protein degradation rates can be directly determined, mRNA half-lives can be inferred (see Section 2.9) [13].

4. Results

4.1. Protein expression dynamics in single cells during the cell cycle

We first used CD-tagging [49] to generate cell lines in which a fusion between Nanoluc, a blasticidin resistance and a SNAP tag (NBS) are internally tagging endogenously-expressed proteins in

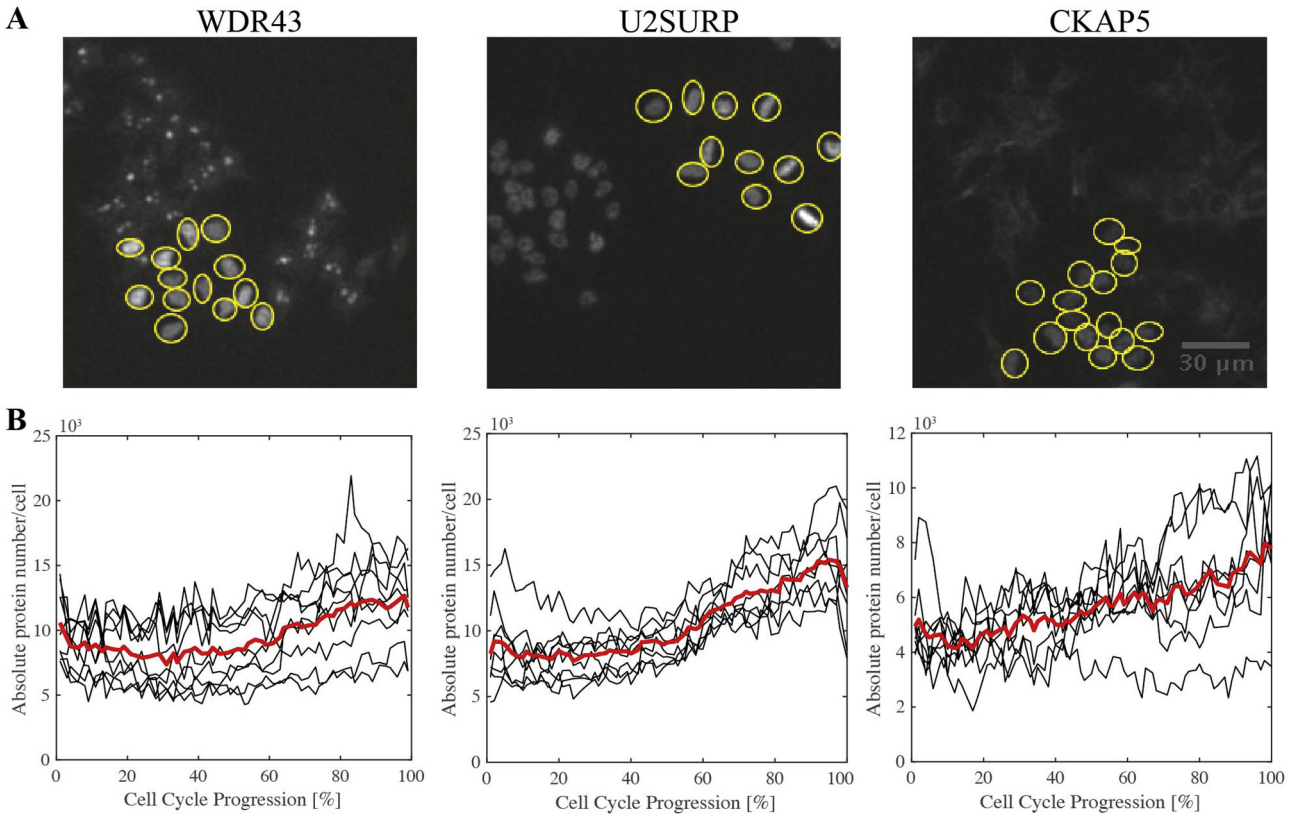

Fig. 2. Protein level fluctuations during the cell cycle. (A) Snapshots from time-lapse recordings for each CD-tagged cell line. Yellow circles: calibration cells used for the signal normalization. (B) Absolute protein copy numbers of *in silico* synchronized single cells quantified from luminescent traces (n = 10). The red line represents the average protein level for each cell line throughout the cell cycle. (For interpretation of the references to color in this figure legend, the reader is referred to the web version of this article.)

mouse ES cells (see Section 2.3). The resulting clonal cell lines were analyzed by 3′RACE to identify the insertion sites (see Section 2.4). We then focused on three different cell lines, in which the NBS tag was fused to WDR43, U2SURP and CKAP5, respectively. These three tagged proteins have different subcellular localizations and functions. WDR43 is a protein localized in nucleoli, which is involved in rRNA processing and ribosome biogenesis; U2SURP is localized in the nucleus and is involved in RNA processing; CKAP is a cytoskeleton-associated protein and plays a role in spindle formation [50–53].

Time-lapse luminescence imaging was then performed in order to measure expression levels of WDR43, U2SURP and CKAP5 at a time resolution of 13–15 min in single cells. In all three cell lines, the tagged proteins were localized as expected (Figs. 2A, and 3A) [50–53]. Subsequently, cells were tracked to measure integrated luminescence intensities over time, which allowed us to quantify absolute protein numbers in single cells for each tracked cell at each time point (see Section 2.5). To quantify protein levels during cell cycle progression, cells were tracked from birth (just after division of the mother cell) to the next division. As shown in Fig. 2B, the three cell lines display variable levels and dynamics of protein expression throughout the cell cycle, with CKAP5 featuring the lowest expression levels and U2SURP the lowest intercellular variability. Note that the drop in observed protein levels at the end of the cell cycle is likely due to rounding up of cells during mitosis, which leads to a loss of focus and thus a decrease in the amount of light collected. We also estimated the error on protein copy number assessment, which was very similar for all three proteins (16.8%, 15.1% and 14.7% for WDR43, U2SURP and CKAP5, respectively). Of note, the relative error is dominated the error on the time independent parameter α (Fig. 1B) and is thus quite stable over time (See Supplementary Information, Section 1, Fig. S1).

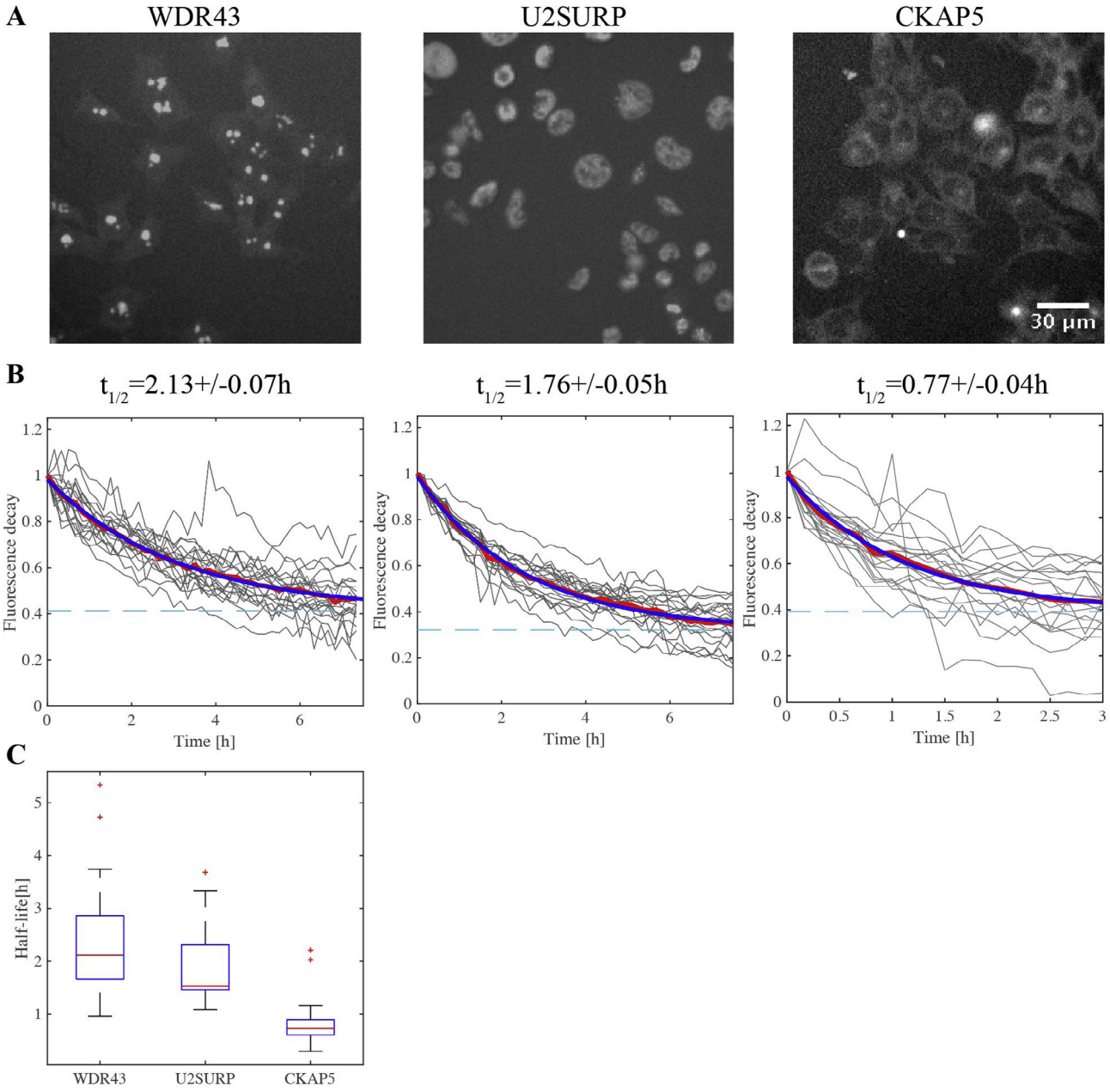

Fig. 3. SNAP tag protein half-life determination. (A) Snapshots from fluorescent time-lapse recordings for each CD-tagged cell lines. (B) Fluorescence signal decays. Red line: average signal decay. Blue line: single exponential fit to the average signal decay (C) Box plots of protein half-life distributions in single cells (n = 20), for each cell line. On each box, the central mark indicates the median value, and the boxes range from the 25th to the 75th percentile. The whiskers extend to the most extreme data points that are not considered as outliers. (For interpretation of the references to color in this figure legend, the reader is referred to the web version of this article.)

Table 2
Average absolute protein synthesis rates per cell cycle ± uncertainty.

Protein name	Protein synthesis rate (S_T) per cell cycle
WDR43	40,200 ± 1600
U2SURP	74,900 ± 2700
CKAP5	102,300 ± 6400

4.2. Determination of protein half-lives and protein synthesis rates

SNAP-tag fluorescence time-lapse imaging was used to measure protein degradation rates in single cells, which allows direct determination of protein half-lives. Briefly, cells were labeled with the SiR-SNAP dye for 30 min, washed thoroughly and imaged for 24 h, at a time resolution of 10 min (Fig. 3A). Since newly synthesized proteins after dye washout are not labeled, this enables measuring protein degradation rates in single cells by monitoring the decay of the fluorescence signal over time. Assuming that the signal decay follows first order exponential dynamics, average protein half-lives for all three proteins can be calculated (Fig. 3B) as described in Section 2.8. Interestingly, we observed large intercellular variability in protein half-lives (Fig. 3C); this variability is unlikely to be due to technical noise related to low fluorescent signal, since the protein expressed at the lowest level (CKAP5) did not display more intercellular variability than WDR43 or U2SURP (Fig. 3C). Importantly, our method can also be used to estimate the average absolute number of proteins synthesized over the cell cycle (Table 2), using absolute protein copy numbers and protein degradation rates that we measured (see Section 2.8, Eqs. (3) and (4)).

4.3. Determination of mRNA half-lives

To allow inducible excision of the NBS tag, we first transduced the CD-tagged cell lines with two lentiviral vectors: i) to express the reverse tetracycline transactivator rtTA3G and ii) to express Cre under the control of a dox-inducible promoter. Upon dox treatment, Cre is expressed and recombines out the NBS tag, resulting in a decay of the signal, which is governed by mRNA half-life, translation rate and protein half-life. In the absence of dox, we did not identify cells decreasing their luminescence signal over time. After dox addition, we observed approximately 10–60% of cells that were gradually losing their luminescent signal, suggesting that the NBS reporter was excised from its integration site. We tracked 20 decaying cells per cell line and each trace was normalized as described in Section 2.5 and absolute protein levels were calculated. To obtain mRNA half-lives, we fitted the combined mRNA and protein decay using Eq. (6), from which we inferred mRNA degradation rate γ_m and that allows to calculate mRNA half-lives (see Section 2.9, Fig. 4).

5. Discussion

In this study we present a novel method allowing quantification of several parameters governing protein expression dynamics in single living cells, including absolute protein quantification at high time resolution and quantitative measurements of protein and mRNA turnover.

5.1. NanoLuc imaging allows highly sensitive monitoring of protein levels over extended time periods

Fluorescent reporters are most widely used for quantification of absolute protein numbers and dynamic protein fluctuations in single cells [17,18,54]. However, they suffer from a number of limitations. First, long maturation times and variable folding efficiency have been shown to lead to data misinterpretation. Second, limited brightness and strong autofluorescence can severely limit their signal-to-noise ratio. Third, phototoxicity limits both the temporal resolution and the total duration of long term imaging experiments [20,55,56]. While luminescent reporters have been widely adopted for dynamical transcriptional and gene expression analysis [13,32,33,57], they have so far not been applied to absolute quantification and protein expression fluctuation measurements of endogenously expressed proteins. NanoLuc (Nluc) is a recently developed luciferase reporter with the brightest bioluminescence reported so far. It is smaller (19 kDa), monomeric and structurally more stable in a wide range of environmental conditions compared to previously used luciferase reporters [58,59]. Therefore, Nluc is an excellent choice as a fusion tag and for sensitive monitoring of proteins in living cells, allowing detection and absolute quantification of proteins at high time resolution and over long periods of time. In the future, it will be interesting to interrogate the sensitivity of Nluc activity in different subcellular compartments to assess its sensitivity to alterations of the chemical environment, such as the low pH of lysosomes.

Gene expression is a stochastic process that leads to phenotypic intercellular variation in an isogenic cell population [4]. Until now, cell-to-cell variability in endogenous protein copy numbers have been mainly studied in microorganisms [60] but there are only

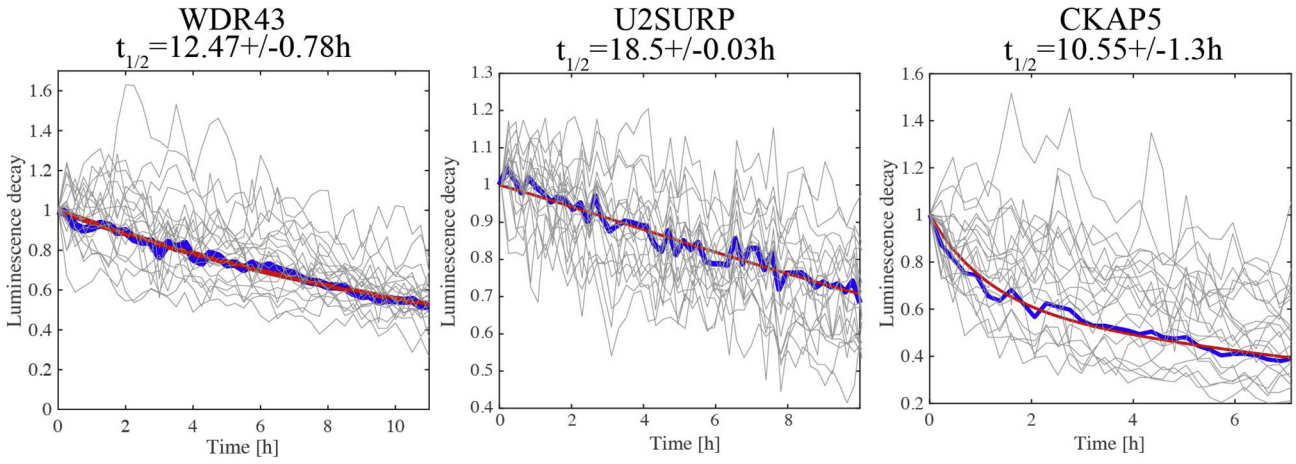

Fig. 4. Combined mRNA and protein decay traces obtained upon Cre recombination. Plots show single cell and averaged decay (in red). The average decay traces were further used for mRNA half-life estimations. (For interpretation of the references to color in this figure legend, the reader is referred to the web version of this article.)

few studies in mammalian cells investigating endogenous proteins dynamics over the cell cycle [15]. The method we report here provides a new approach to explore protein fluctuations in single living mammalian cells for extended time periods. While the observed range of protein expression levels was around 2000–20,000 protein copies per cell, fluctuations of these levels over a few hundred proteins were clearly visible. Such low level fluctuations would arguably not be measurable using fluorescent proteins, which are limited in their sensitivity to a few thousands of proteins per cell [17,18] and suffer from photobleaching and phototoxicity when high temporal resolution imaging in required. Thus, our system represents an excellent choice for absolute copy number quantification of lowly abundant proteins and cell-to-cell variability with high temporal resolution over extended time periods.

5.2. Protein degradation rates show high variability among single cells

The high intercellular variability of gene expression in phenotypically homogeneous cell populations is commonly attributed to variations in transcriptional activity [13,61]. While mRNA degradation rates, translational efficiency, or protein degradation rate can play an important role in determining protein levels [48,62], it is still unclear how these post-transcriptional mechanisms contribute to variability in protein expression levels. Using our single-cell, real-time monitoring of protein degradation rates, we show that WDR43 and U2SURP proteins display large cell-to-cell variability in their protein half-lives (Fig. 3C), suggesting that protein degradation rate is an important contributor to intercellular variation in protein levels. Although there is no evidence that the SNAP tag or Nluc as fusion reporters lead to alteration of endogenous protein stability and internal tagging with fluorescent proteins has also been shown to preserve protein half-lives [15], we cannot exclude they may alter the stability of some proteins. Therefore, while the observed cell-to-cell variability in protein degradation rates is unlikely to be due by a potential alteration of endogenous protein half-life, the average values of the measured half-lives must be interpreted cautiously and may benefit from validation through an independent method. Further studies will be needed to assess how well endogenous protein half-lives are preserved upon internal or N/C-terminal tagging.

5.3. Determination of protein half-lives and absolute protein copy numbers allows to determine absolute protein synthesis rates

The stability and turnover of proteins in cells determines their absolute expression levels and temporal fluctuations, which have important implications in their function [63,64]. Until now, only few studies have attempted to perform such measurements [48]. These studies are mainly based on quantifying relative protein synthesis rates [65,66], or rely on technically challenging approaches to determine absolute values [48,66]. Our method allows to directly calculate absolute protein synthesis rates, knowing the average protein levels and protein degradation rates (Table 2). Importantly, even though alteration of protein half-life by our tag cannot be excluded, any change in degradation rate is accompanied by a proportional change in protein levels at steady state and thus do not affect the estimation of absolute protein synthesis rates.

5.4. mRNA half-life determination

Regulation of mRNA turnover is an important parameter controlling the levels of cellular transcripts and therefore the levels of protein expression, and mRNA half-lives can vary over several orders of magnitude [48]. Here we describe an innovative approach to measuring mRNA decay, which allows instantaneous arrest of the transcription of our internal tag by inducible Cre-mediated excision. Since this does not rely on continuous exposure of cells to drugs or labeled ribonucleotides, it is particularly non-perturbative and allows straightforward quantification of mRNA degradation rates in living cells.

5.5. Future perspectives

In the future, different approaches should allow this method to be extended to multicolor imaging for long term monitoring of several different proteins in the same cell. First, in addition to Nluc, Fluc could be also used as a protein tag in our system. These two proteins can be discriminated using an appropriate set of filters, as shown here in the case of the calibration cell line. Second, recent bright Nanoluc-fluorescent protein fusions allowing bioluminescence resonance energy transfer (BRET) have been described [67–69] potentially allowing multicolor imaging of different proteins simultaneously. Finally, the interrogation of biological processes with both high sensitivity and spatial resolution should also be possible by combining luminescent and fluorescent reporters.

6. Conclusion

Here we describe a novel method allowing to measure absolute protein expression levels, protein half-lives and synthesis rates, as well as mRNA half-lives for endogenously expressed genes. The method relies exclusively on commercially available equipment and reagents, and thus shall be easy to implement in any classical molecular/cellular biology laboratory. The future of biology will increasingly rely on more quantitative measurements, and in this context our approach may significantly contribute to improving the breadth of single cell gene expression analysis.

Acknowledgments

We thank José Artacho from the EPFL BioImaging & Optics Core Facility (EPFL-BIOP) for assistance in imaging and Sara Ancel for her help with generation of cell lines and time-lapse imaging. This work was supported by the Swiss National Science Foundation (grant #PP00P3_144828).

Appendix A. Supplementary data

Supplementary data associated with this article can be found, in the online version, at http://dx.doi.org/10.1016/j.ymeth.2017.04.008.

References

[1] A. McDavid, L. Dennis, P. Danaher, G. Finak, M. Krouse, A. Wang, P. Webster, J. Beechem, R. Gottardo, Modeling bi-modality improves characterization of cell cycle on gene expression in single cells, PLoS Comput. Biol. 10 (7) (2014) e1003696.
[2] C. Zopf, K. Quinn, J. Zeidman, N. Maheshri, Cell-cycle dependence of transcription dominates noise in gene expression, PLoS Comput. Biol. 9 (7) (2013) e1003161.
[3] B. Snijder, R. Sacher, P. Rämö, E.-M. Damm, P. Liberali, L. Pelkmans, Population context determines cell-to-cell variability in endocytosis and virus infection, Nature 461 (7263) (2009) 520–523.
[4] A. Raj, A. van Oudenaarden, Nature, nurture, or chance: stochastic gene expression and its consequences, Cell 135 (2) (2008) 216–226.
[5] J.H. Lee, E.R. Daugharthy, J. Scheiman, R. Kalhor, J.L. Yang, T.C. Ferrante, R. Terry, S.S. Jeanty, C. Li, R. Amamoto, Highly multiplexed subcellular RNA sequencing in situ, Science 343 (6177) (2014) 1360–1363.
[6] J. Moffitt, X. Zhuang, Chapter one-RNA imaging with multiplexed error-robust fluorescence in situ hybridization (MERFISH), Methods Enzymol. 572 (2016) 1–49.
[7] C. Lombard-Banek, S.A. Moody, P. Nemes, Single-cell mass spectrometry for discovery proteomics: quantifying translational cell heterogeneity in the 16-Cell frog (Xenopus) embryo, Angew. Chem. Int. Ed. 55 (7) (2016) 2454–2458.

[8] R.M. Onjiko, S.A. Moody, P. Nemes, Single-cell mass spectrometry reveals small molecules that affect cell fates in the 16-cell embryo, Proc. Natl. Acad. Sci. 112 (21) (2015) 6545–6550.
[9] Y. Lin, C.H. Sohn, C.K. Dalal, L. Cai, M.B. Elowitz, Combinatorial gene regulation by modulation of relative pulse timing, Nature (2015).
[10] D.R. Larson, D. Zenklusen, B. Wu, J.A. Chao, R.H. Singer, Real-time observation of transcription initiation and elongation on an endogenous yeast gene, Science 332 (6028) (2011) 475–478.
[11] M.L. Ferguson, D.R. Larson, Measuring transcription dynamics in living cells using fluctuation analysis, Imaging Gene Expression Methods Protoc. (2013) 47–60.
[12] E. Bertrand, P. Chartrand, M. Schaefer, S.M. Shenoy, R.H. Singer, R.M. Long, Localization of ASH1 mRNA particles in living yeast, Mol. Cell 2 (4) (1998) 437–445.
[13] D.M. Suter, N. Molina, D. Gatfield, K. Schneider, U. Schibler, F. Naef, Mammalian genes are transcribed with widely different bursting kinetics, Science 332 (6028) (2011) 472–474.
[14] P.S. Hoppe, D.L. Coutu, T. Schroeder, Single-cell technologies sharpen up mammalian stem cell research, Nat. Cell Biol. 16 (10) (2014) 919–927.
[15] A. Sigal, R. Milo, A. Cohen, N. Geva-Zatorsky, Y. Klein, Y. Liron, N. Rosenfeld, T. Danon, N. Perzov, U. Alon, Variability and memory of protein levels in human cells, Nature 444 (7119) (2006) 643–646.
[16] D.A. Faddah, H. Wang, A.W. Cheng, Y. Katz, Y. Buganim, R. Jaenisch, Single-cell analysis reveals that expression of nanog is biallelic and equally variable as that of other pluripotency factors in mouse ESCs, Cell Stem Cell 13 (1) (2013) 23–29.
[17] P.S. Hoppe, M. Schwarzfischer, D. Loeffler, K.D. Kokkaliaris, O. Hilsenbeck, N. Moritz, M. Endele, A. Filipczyk, A. Gambardella, N. Ahmed, Early myeloid lineage choice is not initiated by random PU. 1 to GATA1 protein ratios, Nature 535 (7611) (2016) 299–302.
[18] A. Filipczyk, C. Marr, S. Hastreiter, J. Feigelman, M. Schwarzfischer, P.S. Hoppe, D. Loeffler, K.D. Kokkaliaris, M. Endele, B. Schauberger, Network plasticity of pluripotency transcription factors in embryonic stem cells, Nat. Cell Biol. (2015).
[19] A.J. Wollman, M.C. Leake, Millisecond single-molecule localization microscopy combined with convolution analysis and automated image segmentation to determine protein concentrations in complexly structured, functional cells, one cell at a time, Faraday Discuss. 184 (2015) 401–424.
[20] R.H. Newman, M.D. Fosbrink, J. Zhang, Genetically encodable fluorescent biosensors for tracking signaling dynamics in living cells, Chem. Rev. 111 (5) (2011) 3614–3666.
[21] B. Baliga, A. Pronczuk, H. Munro, Mechanism of cycloheximide inhibition of protein synthesis in a cell-free system prepared from rat liver, J. Biol. Chem. 244 (16) (1969) 4480–4489.
[22] A. Belle, A. Tanay, L. Bitincka, R. Shamir, E.K. O'Shea, Quantification of protein half-lives in the budding yeast proteome, Proc. Natl. Acad. Sci. 103 (35) (2006) 13004–13009.
[23] O. Bensaude, Inhibiting eukaryotic transcription. Which compound to choose? How to evaluate its activity? Which compound to choose? How to evaluate its activity?, Transcription 2 (3) (2011) 103–108
[24] H. Tani, R. Mizutani, K.A. Salam, K. Tano, K. Ijiri, A. Wakamatsu, T. Isogai, Y. Suzuki, N. Akimitsu, Genome-wide determination of RNA stability reveals hundreds of short-lived noncoding transcripts in mammals, Genome Res. 22 (5) (2012) 947–956.
[25] C.-L. Dai, J. Shi, Y. Chen, K. Iqbal, F. Liu, C.-X. Gong, Inhibition of protein synthesis alters protein degradation through activation of protein kinase B (AKT), J. Biol. Chem. 288 (33) (2013) 23875–23883.
[26] C. Deluz, E.T. Friman, D. Strebinger, A. Benke, M. Raccaud, A. Callegari, M. Leleu, S. Manley, D.M. Suter, A role for mitotic bookmarking of SOX2 in pluripotency and differentiation, Genes Dev. (2016).
[27] J.H. Kim, S.-R. Lee, L.-H. Li, H.-J. Park, J.-H. Park, K.Y. Lee, M.-K. Kim, B.A. Shin, S.-Y. Choi, High cleavage efficiency of a 2A peptide derived from porcine teschovirus-1 in human cell lines, zebrafish and mice, PLoS One 6 (4) (2011) e18556.
[28] A. Sigal, R. Milo, A. Cohen, N. Geva-Zatorsky, Y. Klein, I. Alaluf, N. Swerdlin, N. Perzov, T. Danon, Y. Liron, Dynamic proteomics in individual human cells uncovers widespread cell-cycle dependence of nuclear proteins, Nat. Methods 3 (7) (2006) 525–531.
[29] J.W. Jarvik, S. Adler, C. Telmer, V. Subramaniam, A. Lopez, CD-tagging: a new approach to gene and protein discovery and analysis, Biotechniques 20 (5) (1996) 896–904.
[30] D.J. Park, A.J. Pask, M.B. Renfree, J. Graves, 3'RACE walking along a large cDNA employing tiered suppression PCR, BioTechniques 34 (4) (2003) 750-2–754-6.
[31] M. Nagaoka, U. Koshimizu, S. Yuasa, F. Hattori, H. Chen, T. Tanaka, M. Okabe, K. Fukuda, T. Akaike, E-cadherin-coated plates maintain pluripotent ES cells without colony formation, PLoS One 1 (1) (2006) e15.
[32] M. Izumo, C.H. Johnson, S. Yamazaki, Circadian gene expression in mammalian fibroblasts revealed by real-time luminescence reporting: temperature compensation and damping, Proc. Natl. Acad. Sci. 100 (26) (2003) 16089–16094.
[33] D.K. Welsh, S.-H. Yoo, A.C. Liu, J.S. Takahashi, S.A. Kay, Bioluminescence imaging of individual fibroblasts reveals persistent, independently phased circadian rhythms of clock gene expression, Curr. Biol. 14 (24) (2004) 2289–2295.
[34] S.J. Duellman, W. Zhou, P. Meisenheimer, G. Vidugiris, J.J. Cali, P. Gautam, K. Wennerberg, J. Vidugiriene, Bioluminescent, Nonlytic, Real-Time Cell Viability Assay and Use in Inhibitor Screening, ASSAY Drug Dev. Technol. 13 (8) (2015) 456–465.
[35] P. Zhou, Determining protein half-lives, Signal Transduction Protocols, 2004, pp. 67–77.
[36] M.K. Doherty, D.E. Hammond, M.J. Clague, S.J. Gaskell, R.J. Beynon, Turnover of the human proteome: determination of protein intracellular stability by dynamic SILAC, J. Proteome Res. 8 (1) (2008) 104–112.
[37] M. Mann, Functional and quantitative proteomics using SILAC, Nat. Rev. Mol. Cell Biol. 7 (12) (2006) 952–958.
[38] H.-C.S. Yen, Q. Xu, D.M. Chou, Z. Zhao, S.J. Elledge, Global protein stability profiling in mammalian cells, Science 322 (5903) (2008) 918–923.
[39] N. Geva-Zatorsky, I. Issaeva, A. Mayo, A. Cohen, E. Dekel, T. Danon, L. Cohen, Y. Liron, U. Alon, E. Eden, Using bleach-chase to measure protein half-lives in living cells, Nat. Protoc. 7 (4) (2012) 801–811.
[40] A. Juillerat, T. Gronemeyer, A. Keppler, S. Gendreizig, H. Pick, H. Vogel, K. Johnsson, Directed evolution of O 6-alkylguanine-DNA alkyltransferase for efficient labeling of fusion proteins with small molecules in vivo, Chem. Biol. 10 (4) (2003) 313–317.
[41] A. Keppler, S. Gendreizig, T. Gronemeyer, H. Pick, H. Vogel, K. Johnsson, A general method for the covalent labeling of fusion proteins with small molecules in vivo, Nat. Biotechnol. 21 (1) (2003) 86–89.
[42] A. Keppler, H. Pick, C. Arrivoli, H. Vogel, K. Johnsson, Labeling of fusion proteins with synthetic fluorophores in live cells, Proc. Natl. Acad. Sci. U.S.A. 101 (27) (2004) 9955–9959.
[43] T. Gronemeyer, C. Chidley, A. Juillerat, C. Heinis, K. Johnsson, Directed evolution of O6-alkylguanine-DNA alkyltransferase for applications in protein labeling, Protein Eng. Des. Sel. 19 (7) (2006) 309–316.
[44] D. Srikun, A.E. Albers, C.I. Nam, A.T. Iavarone, C.J. Chang, Organelle-targetable fluorescent probes for imaging hydrogen peroxide in living cells via SNAP-Tag protein labeling, J. Am. Chem. Soc. 132 (12) (2010) 4455–4465.
[45] D. Maurel, L. Comps-Agrar, C. Brock, M.-L. Rives, E. Bourrier, M.A. Ayoub, H. Bazin, N. Tinel, T. Durroux, L. Prézeau, Cell-surface protein-protein interaction analysis with time-resolved FRET and snap-tag technologies: application to GPCR oligomerization, Nat. Methods 5 (6) (2008) 561–567.
[46] K. Bojkowska, F.S. de Sio, I. Barde, S. Offner, S. Verp, C. Heinis, K. Johnsson, D. Trono, Measuring in vivo protein half-life, Chem. Biol. 18 (6) (2011) 805–815.
[47] W.T. Melvin, H.B. Milne, A.A. Slater, H.J. Allen, H.M. Keir, Incorporation of 6-Thioguanosine and 4-Thiouridine into RNA, Eur. J. Biochem. 92 (2) (1978) 373–379.
[48] B. Schwanhäusser, D. Busse, N. Li, G. Dittmar, J. Schuchhardt, J. Wolf, W. Chen, M. Selbach, Global quantification of mammalian gene expression control, Nature 473 (7347) (2011) 337–342.
[49] J. Jarvik, G. Fisher, C. Shi, L. Hennen, C. Hauser, S. Adler, P. Berget, In vivo functional proteomics: mammalian genome annotation using CD-tagging, Biotechniques 33 (4) (2002) 852–867.
[50] Y.-T. Yu, M.-D. Shu, A. Narayanan, R.M. Terns, M.P. Terns, J.A. Steitz, Internal modification of U2 small nuclear (snRNA) occurs in nucleoli of Xenopus oocytes, J. Cell Biol. 152 (6) (2001) 1279–1288.
[51] M.A. Jarboui, C. Bidoia, E. Woods, B. Roe, K. Wynne, G. Elia, W.W. Hall, V.W. Gautier, Nucleolar protein trafficking in response to HIV-1 Tat: rewiring the nucleolus, PLoS One 7 (11) (2012) e48702.
[52] K. Wada, M. Sato, N. Araki, M. Kumeta, Y. Hirai, K. Takeyasu, K. Furukawa, T. Horigome, Dynamics of WD-repeat containing proteins in SSU processome components, Biochem. Cell Biol. 92 (3) (2014) 191–199.
[53] V.P. Francone, M.J. Maggipinto, L.D. Kosturko, E. Barbarese, The microtubule-associated protein tumor overexpressed gene/cytoskeleton-associated protein 5 is necessary for myelin basic protein expression in oligodendrocytes, J. Neurosci. Res. 27 (29) (2007) 7654–7662.
[54] A. Filipczyk, K. Gkatzis, J. Fu, P.S. Hoppe, H. Lickert, K. Anastassiadis, T. Schroeder, Biallelic expression of nanog protein in mouse embryonic stem cells, Cell Stem Cell 13 (1) (2013) 12–13.
[55] J.S. Verdaasdonk, J. Lawrimore, K. Bloom, Determining absolute protein numbers by quantitative fluorescence microscopy, Methods Cell Biol. 123 (2014) 347.
[56] T. Schroeder, Long-term single-cell imaging of mammalian stem cells, Nat. Methods 8 (4s) (2011) S30–S35.
[57] A. Mazo-Vargas, H. Park, M. Aydin, N.E. Buchler, Measuring fast gene dynamics in single cells with time-lapse luminescence microscopy, Mol. Biol. Cell 25 (22) (2014) 3699–3708.
[58] A.E. Masser, G. Kandasamy, J.M. Kaimal, C. Andréasson, Luciferase NanoLuc as a reporter for gene expression and protein levels in Saccharomyces cerevisiae, Yeast (2016).
[59] M.P. Hall, J. Unch, B.F. Binkowski, M.P. Valley, B.L. Butler, M.G. Wood, P. Otto, K. Zimmerman, G. Vidugiris, T. Machleidt, Engineered luciferase reporter from a deep sea shrimp utilizing a novel imidazopyrazinone substrate, ACS Chem. Biol. 7 (11) (2012) 1848–1857.
[60] Y. Taniguchi, P.J. Choi, G.-W. Li, H. Chen, M. Babu, J. Hearn, A. Emili, X.S. Xie, Quantifying E. coli proteome and transcriptome with single-molecule sensitivity in single cells, Science 329 (5991) (2010) 533–538.
[61] A. Raj, C.S. Peskin, D. Tranchina, D.Y. Vargas, S. Tyagi, Stochastic mRNA synthesis in mammalian cells, PLoS Biol. 4 (10) (2006) e309.

Please cite this article in press as: A. Mandic et al., Methods (2017), http://dx.doi.org/10.1016/j.ymeth.2017.04.008

[62] M. Jovanovic, M.S. Rooney, P. Mertins, D. Przybylski, N. Chevrier, R. Satija, E.H. Rodriguez, A.P. Fields, S. Schwartz, R. Raychowdhury, Dynamic profiling of the protein life cycle in response to pathogens, Science 347 (6226) (2015) 1259038.
[63] I. Imayoshi, A. Isomura, Y. Harima, K. Kawaguchi, H. Kori, H. Miyachi, T. Fujiwara, F. Ishidate, R. Kageyama, Oscillatory control of factors determining multipotency and fate in mouse neural progenitors, Science 342 (6163) (2013) 1203–1208.
[64] J.E. Purvis, K.W. Karhohs, C. Mock, E. Batchelor, A. Loewer, G. Lahav, P53 dynamics control cell fate, Science 336 (6087) (2012) 1440–1444.
[65] M. Selbach, B. Schwanhäusser, N. Thierfelder, Z. Fang, R. Khanin, N. Rajewsky, Widespread changes in protein synthesis induced by microRNAs, Nature 455 (7209) (2008) 58–63.
[66] B. Schwanhäusser, M. Gossen, G. Dittmar, M. Selbach, Global analysis of cellular protein translation by pulsed SILAC, Proteomics 9 (1) (2009) 205–209.
[67] C.G. England, E.B. Ehlerding, W. Cai, NanoLuc: a small luciferase is brightening up the field of bioluminescence, Bioconjugate Chem. 27 (5) (2016) 1175–1187.
[68] E. Goyet, N. Bouquier, V. Ollendorff, J. Perroy, Fast and high resolution single-cell BRET imaging, Sci. Rep. 6 (2016).
[69] J. Yang, D. Cumberbatch, S. Centanni, S.-Q. Shi, D. Winder, D. Webb, C.H. Johnson, Coupling optogenetic stimulation with NanoLuc-based luminescence (BRET) Ca++ sensing, Nat. Commun. 7 (2016) 13268.